Appl. Phys. B 73, 489–493 (2001)
DOI: 10.1007/s003400100683

Applied Physics B
Lasers and Optics

H. MENDIS[1,*]
A. MITCHELL[1,✉]
I. BELSKI[1]
M. AUSTIN[1]
O.A. PEVERINI[2,**]

Design, realisation and analysis of an apodised, film-loaded acousto-optic tunable filter

[1] School of Electrical and Computer Systems Engineering, RMIT University, Melbourne, Australia
[2] Research Institute on Computer and Telecommunication Engineering, National Research Council of Italy (CNR), Politecnico di Torino, 10129 Torino, Italy

Received: 18 May 2001/Revised version: 7 August 2001
Published online: 23 October 2001 •

ABSTRACT The design and realisation of a SiO_2 film-loaded Ti : $LiNbO_3$ integrated acousto-optic tunable filter are presented. An optimised Hamming apodisation is achieved through introducing an angular offset between the acoustic and optical waveguides along with carefully placed acoustic absorbers. The realised device has a 20-mm acoustic interaction length and achieves a 3-dB linewidth of 1.8 nm with 19-dB sidelobe suppression. The realised device is highly efficient, requiring a RF drive power of only 10 mW to achieve complete polarisation conversion. The enhanced drive efficiency of the device is analysed using both acoustic and optical mode analysis. Based on this analysis, possible explanations for the improved behaviour are presented and directions that may lead to further enhancements are discussed.

PACS 42.79.Jq; 42.82.Gw

1 Introduction

Integrated acousto-optical tunable filters (IAOTFs) are attractive devices for wavelength-division multiplexing (WDM) optical communication systems [1] and also offer potential for use in bio-medical sensing applications [2]. Recently, efforts to migrate IAOTF implementations from Ti-diffused $LiNbO_3$ [3] to film-loaded acoustic waveguides, which allow more flexible control of acoustic mode confinement, have been reported [4]. The current state-of-the-art IAOTF devices are implemented for a 0.8-nm channel-spaced WDM system using multi-folded stages of tilted SiO_2 films with 60 wt % InSn acoustic waveguides on $LiNbO_3$ [5].

A film-loaded IAOTF is depicted in Fig. 1. The application of a RF electric signal to the interdigital transducer electrodes will cause a surface acoustic wave (SAW) to be generated due to the piezoelectric properties of the $LiNbO_3$ substrate. A strip of reduced acoustic velocity material forms a waveguide for the generated SAW along the length of the device. The stress produced by the presence of the SAW on the $LiNbO_3$ surface causes a perturbation in the optical properties of the material. This perturbation can be used to couple the orthogonal TE and TM polarised optical modes propagating in the titanium-diffused optical waveguide beneath the SAW guide.

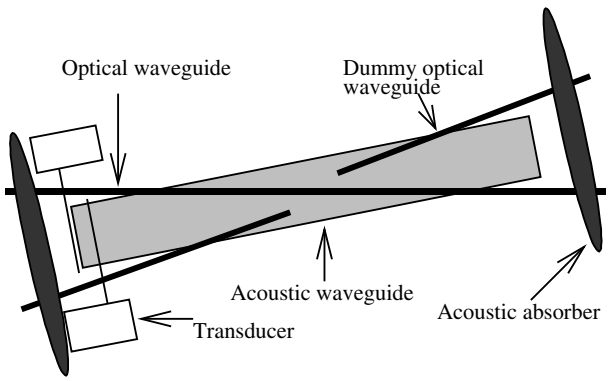

FIGURE 1 Film-loaded integrated acousto-optic tunable filter (IAOTF) structure

Since the stress caused by the SAW is periodic, the optical perturbation is also periodic and thus acts much like an optical grating. Hence, depending on the difference in propagation velocities of the TE and TM polarised optical modes, if the optical wavelength and the acoustic period meet a phase-matching condition, the TE and TM modes will be strongly coupled. For a particular SAW period only a single optical wavelength will meet this phase-matching condition and thus the particular wavelength that has its polarisation converted may be precisely controlled via the RF applied to the transducer. If the input optical signal is of a single polarisation, a polarisation splitter at the output allows the converted wavelength to be dissociated from the other wavelengths.

The resolution and rejection of any filter will largely be determined by the filter apodisation. Many AOTF apodisations have been proposed; however it can be shown that the optimised Hamming apodisation function offers the best compromise between linewidth and sidelobe level [3].

Methods to implement these apodisations in AOTF devices have also been proposed [3, 6]. Some of these techniques can introduce phase variations in the acoustic profile along the path of the optical waveguide, which may result

✉ Fax: +613/9662-1921, E-mail:arnan@bilby.co.rmit.edu.au
*_Present address_: School of Electrical and Computer Systems Engineering, GPO Box 2476V, RMIT University, Victoria 3001, Australia. E-mail: heyshan.mendis@rmit.edu.au
**_Present address:_ IRITI-CNR, Corso Duca degli Abruzzi 24, 10129 Torino, Italy. E-mail: peverini@athena.polito.it

in asymmetry in the filter response and poor sidelobe suppression. Apodising the acousto-optic interaction through use of an angular offset between the acoustic and optical waveguides ensures a constant acoustic phase along the optical path and thus is more likely to provide an optimised filter response. When the acoustic waveguide is formed using a Ti-diffused cladding and the optical waveguide is formed using a Ti-diffused core, it can be impractical to arrange angular offset apodisation as it is difficult to define the optical waveguide outside of the undiffused acoustic guiding region. Strip-loaded acoustic waveguides have a clear advantage in this respect.

This investigation thus focuses on the realisation of an optimised Hamming apodised AOTF through use of an angular offset between the acoustic and optical waveguides. First, in Sect. 2, the acoustic properties of several thin films are analysed to determine which film will be most suitable for strip loading. Based on this analysis, test structures of SiO_2 strip-loaded SAW guides are fabricated on a $LiNbO_3$ substrate to experimentally verify the SAW velocity and attenuation. Section 3 then utilises the experimentally determined SAW guide properties in conjunction with a beam-propagation method (BPM) and coupled-mode-equation models to predict the integrated AOTF response. This modeling enables the design of the SAW guide geometry and relative placement of acoustic and optical waveguides to provide an optimised filter response.

The realisation of the designed filter is described in Sect. 4 along with the measured performance of this device. It is found to offer a reasonably narrow linewidth and good sidelobe suppression, comparing well with predictions. Of particular interest is the enhanced efficiency of the device. Section 5 presents a theoretical analysis of the interaction between the guided acoustic and optical modes in order to better understand the factors contributing to efficient conversion. Drawing on this analysis, several possible avenues for the improvement of the realised device are suggested.

2 Film-loaded SAW guide characterisation

The propagation characteristics of the SAW mode depend on the acoustic velocity difference between the bare $LiNbO_3$ cladding and the film-loaded $LiNbO_3$ guide. Figure 2 presents the velocity difference modelled for SiO_2, MgO, ZnO and AlN films on $LiNbO_3$ using specialised software [6]. This modelling demonstrates that through careful selection of strip material and thickness, a wide range of core acoustic velocities are available. Although films offering high acoustic velocity contrast (such as ZnO) may offer more tightly confined SAW propagation, we have chosen to use SiO_2 for this work. This material offers a moderate reduction in acoustic velocity in the guiding region, very similar to that which can be achieved through Ti diffusion [3, 6], and is routinely produced in our laboratory.

To verify that the acoustic velocity was as predicted in Fig. 2 and to ensure that the acoustic propagation loss was sufficiently low, a SAW test structure was fabricated [7]. The geometry of this test structure is presented in Fig. 3.

The transmitting transducer (T_x) launches acoustic waves along the strip guide in both directions. These acoustic waves

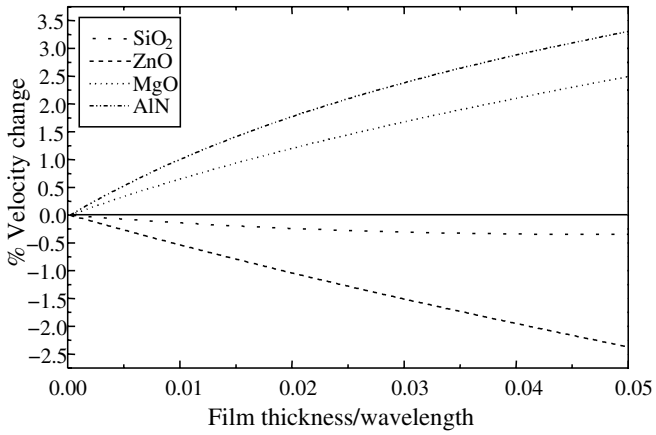

FIGURE 2 SAW velocity change for different films

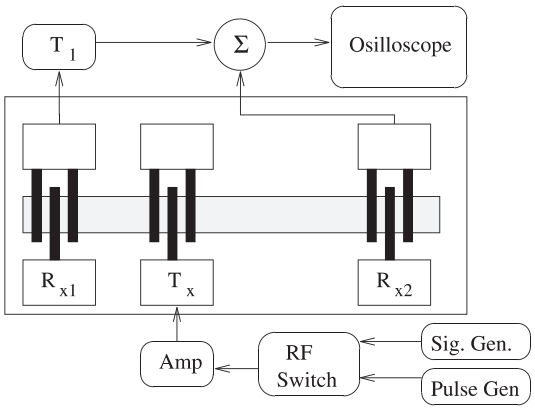

FIGURE 3 SAW velocity-measurement setup

travel two different distances (d_1 and d_2) before being detected at two receiver transducers (R_{x1} and R_{x2} respectively). The input signal is a pulse-modulated tone and the two outputs are summed and displayed on an oscilloscope.

A time delay (T_1) was introduced between the two received signals (as shown in Fig. 3) to approximately compensate for the path difference and then the frequency of the tone was carefully adjusted until the two received signals interfered destructively. The phase velocity V_p was then found by substituting the frequency of cancellation f_{null} into (1):

$$V_p = \frac{2 f_{null}(d_2 - d_1)}{(2i+1)} , \tag{1}$$

where i is an integer.

To fabricate the test structure, the SiO_2 film was deposited using a RF magnetron sputter system using a 99.99% purity SiO_2 target. The chamber was evacuated to a base pressure of 2×10^{-5} Torr and the sample temperature was maintained at 140 °C. A gas mixture of 1 : 9 O_2 : Ar at 1×10^{-2} Torr was introduced and excited with a RF power of 160 W for 30 min to produce a 0.38-μm-thick film. A strip of 80-μm width was then patterned on the surface by masking and etching with HF. The transducer consisted of 20 finger pairs with a 20.8-μm period and was fabricated using an evaporated 200 Å : 300 Å : 500 Å Ti : Ni : Au metallisation to achieve low conductor loss and good adhesion. Au wire bonding was used to connect the transducer to a 150-nH inductor and a 3–20-pF tunable capacitor matching network.

Using the technique described above, the phase velocity of the 80-μm-wide, 0.38-μm-thick SiO_2 strip-loaded SAW guide was found to be 3685 ms^{-1} and the $LiNbO_3$ velocity to be 3700 ms^{-1} at 174.5 MHz. The error in this measurement is estimated to be around $\pm 1\,ms^{-1}$. The SAW attenuation at this frequency was estimated to be 1.75 dB cm^{-1} by comparing the amplitudes of the signals received at R_{x1} and R_{x2} and the corresponding path-length difference.

3 IAOTF response modelling

Having established the propagation characteristics of the SiO_2 strip-loaded SAW guide in Sect. 2, it was possible to use the experimentally verified data to determine the arrangement of acoustic and optical waveguides that offers the optimum wavelength-filter profile.

The evolution of the acoustic signal was modelled using a beam-propagation method model [8, 9]. The resulting polarisation conversion was modelled by recording the acoustic intensity along the optical waveguide (see Fig. 1) and then using coupled-mode theory [10] to determine the polarisation conversion.

The angular offset between the optical waveguide and the SAW guide characterised in Sect. 2 was optimised to achieve an acoustic intensity profile that approximated an optimised Hamming weighting function. During this analysis it was found that a second dummy optical waveguide (as shown in Fig. 1) was needed to maintain symmetry of the acoustic amplitude and sustain good symmetric sidelobe suppression.

The acoustic amplitude profile and corresponding filter characteristics predicted for the 80-μm-wide, 20-mm-long SAW guide at several angular offsets are presented in Fig. 4 and Fig. 5 respectively. An input polarisation extinction ratio of 25 dB is assumed.

From Fig. 5 it is evident that an offset of 0.55° offers the narrowest linewidth, whilst maintaining a low sidelobe level.

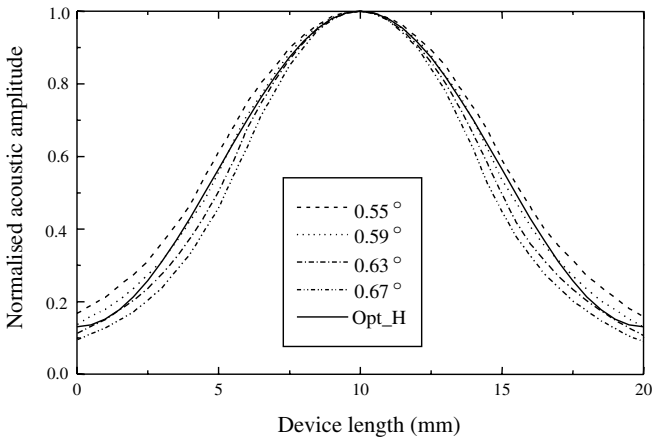

FIGURE 4 Acoustic amplitude for different interaction angles

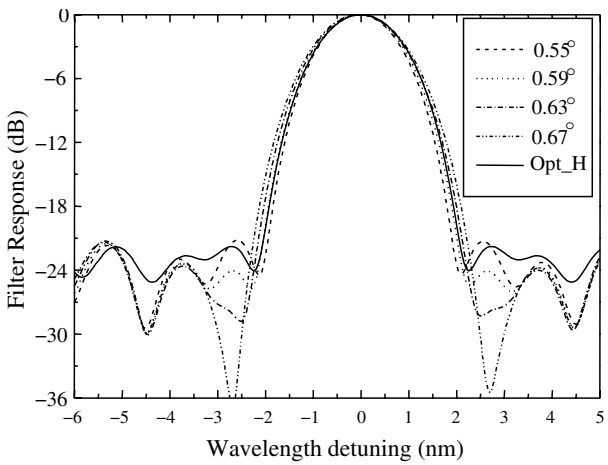

FIGURE 5 Filter response for different interaction angles

4 Film-loaded IAOTF realisation and results

Based on the predictions of Sect. 3, IAOTF devices were fabricated with a 0.38-μm-thick SiO_2 film SAW guide of width 80 μm at an angular offset of 0.55° to the optical waveguide. Acoustic absorbers were placed a short distance from either end of the SAW guide (as depicted in Fig. 1) to truncate the acoustic amplitude profile at its extremities.

It is important for good coupling efficiency and extinction that the TE and TM modes of the optical waveguide are of as similar cross-sectional distributions as possible and that they propagate with the same attenuation. Several experiments were conducted by varying the diffusion temperature and the Ti-strip thickness to produce optical waveguides with TE and TM modes of similar characteristics. The final parameters used were 7-μm-wide, 1000 Å-thick Ti strip diffused for 8 h at 1050 °C.

An optical carrier, supplied by a tunable laser, was polarised using a fibre polarisation controller and then butt-coupled to the IAOTF device. An amplified RF tone at 171 MHz was applied to the transducer, corresponding to an optical conversion wavelength of 1560 nm. The optical output was imaged through a crossed polariser onto an optical power meter. The wavelength of the tunable laser was varied from 1554 to 1565 nm and the optical power transmitted through crossed polarisers was recorded and is presented in Fig. 6. The unconverted power is also shown in Fig. 6, demonstrating that low cross-talk is achieved.

This 20-mm-long device achieves a 3-dB linewidth of 1.8 nm and a sidelobe level of −19 dB. This response compares well to that predicted in Fig. 5 although some slight asymmetry is evident. This asymmetry is most likely caused by small inhomogeneities in the SAW guide and the optical waveguide along the length of the device. The sidelobe level of −19 dB is respectable but falls short of the ideal < -22 dB level predicted for the optimised Hamming apodisation. This shortcoming may be attributed to the non-ideal polarisation extinction ratio at the device input of only 25 dB. It is believed that improvement of this input polarisation control through the use of an integrated optical polarisation splitter would yield further sidelobe-level reduction.

The RF drive power required for maximum conversion of the central optical wavelength was only 10 mW, which is significantly lower than the ≥ 50 mW required by previously reported Ti-diffused geometries [11]. This enhanced conversion efficiency was an important and surprising result. Improving the conversion efficiency is of benefit to system integration for communications and compact spectroscopic applications, in

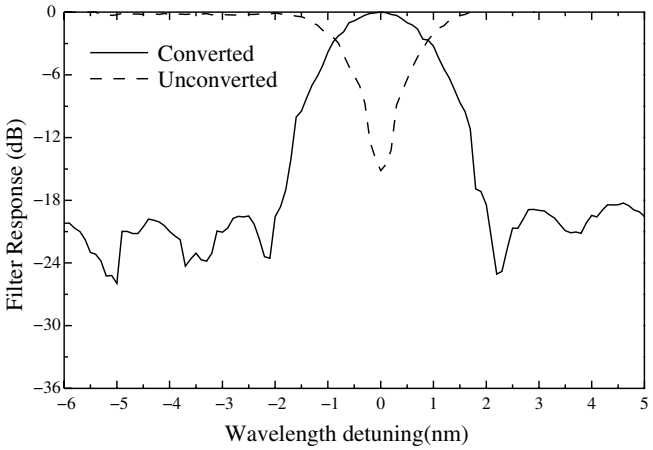

FIGURE 6 Filtered and unfiltered responses at 171 MHz and centre wavelength of 1560 nm

terms of both a reduced impact on the overall power budget for the system and probably more importantly a significant reduction in the heat generated by the device. In order to better understand the observed efficiency, further theoretical analysis of the interaction of the acoustic and optical modes was conducted.

5 Discussion of acousto-optic conversion efficiency

It is proposed that the conversion efficiency is determined by three key aspects of the AOTF device: (i) efficient electro-mechanical coupling at the launching transducer; (ii) the confinement of the acoustic guide and its alignment with the optical modes and (iii) the overlap of the TE and TM polarised optical modes. A discussion of each of these effects, whether they contribute to the the observed efficiency of the current device and how they might be utilised to improve the efficiency of future devices, is presented in the following subsections.

5.1 *Electro-mechanical efficiency at the transducer*

The electro-mechanical coupling coefficient, K, of the transducer is approximately given as [12]

$$K^2 \propto \frac{2(V_\mathrm{f} - V_\mathrm{m})}{V_\mathrm{f}} \,. \tag{2}$$

Here V_f and V_m are the free-material and metallised acoustic wave velocity respectively. According to the results of Sect. 2, the acoustic velocity of a 0.38-μm-thick SiO_2 film and bare $LiNbO_3$ differ by less than 0.3%. The difference between the acoustic velocity of metallised SiO_2 and $LiNbO_3$ should also be small and so the electro-mechanical efficiency should be similar between the strip-loaded and diffused acoustic waveguide transducers. Further, the transducer used in the strip-loaded device reported here was very similar to that reported in [11], having a 20-finger-pair variable capacitor and using a series inductor for impedance matching. Thus it is unlikely that an improvement in efficiency of the order observed could result from enhanced transducer performance.

In this device the transducer was not optimised to compensate for the acoustic walk-off [13]. A slight rotation of the transducer has been shown to improve the efficiency of launching acoustic waves in diffused SAW guides [14], and it is expected that a similar improvement could result when applied to the strip-loaded guide under investigation. Other possibilities that could be pursued to improve efficiency include implementation of unidirectional transducers and examination of the efficiency with which the transducers launch the fundamental mode of the SAW guide.

5.2 *Acousto-optic efficiency*

Another significant factor contributing to the filter conversion efficiency is the efficiency of the interaction between the optical modes and the acoustic perturbation.

The coupling coefficient in X-cut Y-propagating $LiNbO_3$ devices can be quite accurately modelled using the following approximation [15]:

$$k \approx k_{xz} = \frac{\omega}{8P_\mathrm{SAW}} \int\int (E_x^\mathrm{TM})^* \Delta\varepsilon_{xz} E_z^\mathrm{TE} \mathrm{d}x\mathrm{d}y \,. \tag{3}$$

Here E_x^TM and E_z^TE are the electric field components of the TM and TE optical modes directed along the crystal X and Z axes respectively and $\Delta\varepsilon_{xz}$ is the perturbation in the permeability that couples the TE and TM optical modes. This is approximately proportional to the strain and electric field components of the SAW in the X direction.

To ensure the most efficient polarisation conversion, the X-directed SAW distribution profile must be a good match to the optical modes. It is thus proposed that a tightly confined acoustic mode would enhance efficiency by causing more acoustic power to be coincident with the propagating optical modes.

The current strip-loaded waveguide does not have a tightly confined acoustic mode, having a similar ratio of guide to cladding acoustic velocity as the diffused device in [16]. The strip-loaded waveguide width of 80 μm is slightly narrower than the 100-μm width of [11]; however this is unlikely to cause the observed improvement in efficiency.

A further enhancement of the efficiency could be sought by significantly increasing the confinement of the acoustic mode so that its width was closer to that of the optical modes. This could be done through the use of an alternative material such as ZnO for the strip waveguide as suggested in Sect. 2. Another approach is to further load the SiO_2 strip waveguide with a thin layer of dense material. Seino et al. [4] have used an InSn-loaded SiO_2 film and significantly narrower strip guide widths to attain a conversion power of only 5 mW. To maintain the same apodisation with a more tightly confined SAW it would be necessary to reduce the angular offset significantly.

5.3 *TE and TM optical mode overlap*

It is evident from (3) that it is not only important for the acoustic mode to match the optical modes, it is also very important that the TE and TM optical modes match each other. Careful experimentation was conducted to ensure that the TE and TM modes were as similar as possible, both in terms of field profile and also in terms of propagation loss to maximise the possible extinction. The measured power-normalised field profiles for the TE and TM optical modes are presented in

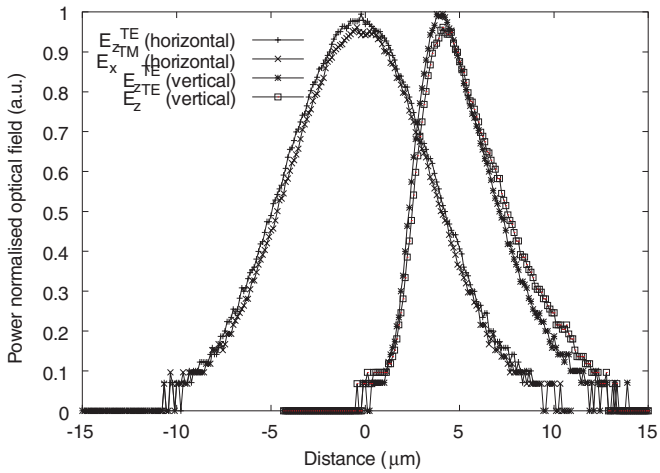

FIGURE 7 Measured power-normalised fields for the TE and TM optical modes in both horizontal and vertical directions

Fig. 7. The field distributions of the two optical modes are evidently very closely matched.

It is thus suggested that most of the improvement in observed conversion efficiency is due to the good overlap between the TE and TM optical modes. It will therefore be worth attempting to implement some of the techniques described above to further improve the conversion efficiency. An investigation of applying these techniques to the present device is currently under way.

6 Conclusion

In this investigation we have demonstrated an integrated acousto-optic tunable filter utilising a SiO_2 film-loaded SAW guide at an angular offset to the optical path to implement an optimised Hamming apodisation. The characteristics of the film-loaded SAW guide in isolation have been accurately modelled and experimentally verified. The strip-loaded SAW guide has been used in the realisation of an apodised SiO_2 film-loaded integrated acousto-optic tunable filter device and achieves a 19-dB sidelobe suppression and a 3-dB linewidth of 1.8 nm for a 20-mm acoustic interaction length. It is believed that the sidelobe-level suppression and the filter linewidth could be improved with the incorporation of more precise polarisation control, and extension of the acousto-optic interaction-region length.

The demonstrated device is highly efficient, requiring only 10 mW of RF power for complete optical polarisation conversion. A detailed discussion of the factors determining conversion efficiency in this device has been presented and suggests that this observed efficiency is due to good matching between the TE and TM optical modes. Several alternative avenues for further improvement of the device efficiency have been identified and efforts to implement these proposed techniques are currently under way.

ACKNOWLEDGEMENTS The authors wish to thank Dr. Harald Herrmann, University of Paderborn, Germany, for the valuable discussion and feedback on this work and Mr. Kourosh Kalantar-zadeh for his assistance in film deposition.

REFERENCES

1 W. Sohler, H. Herrmann, K. Schäfer: 'Tunable Acousto-optical Filters, Multiplexers and Lasers in $LiNbO_3$'. In Dig. IEEE/LEOS Summer Top. Meet. Vert.-Cavity Lasers, August 1997, pp. 44–45
2 N. Gupta, R. Dahmani: 'Acousto-optic Sensing and Imaging for Biomedical Applications'. In Proc. 19th Annu. Int. Conf. IEEE Eng. Med. Biol. Soc., October 1997, Vol. 2, pp. 702–703
3 A. Kar-Roy, C.S. Tsai: J. Lightwave Technol. **12**, 977 (1994)
4 M. Seino, T. Nakazawa, M. Doi, S. Taniguchi, Y. Takasu: 'Low Sidelobe and Low Insertion Loss Ti:$LiNbO_3$ AOTF'. In IEEE/LEOS 1997 Summer Top. Meet., Montreal, August 1997
5 H. Miyata, Y. Kaito, Y. Kai, H. Onaka, T. Nakazawa, M. Doi, M. Seino, T. Chikama, Y. Kotaki, K. Wakao, M. Komiyama, T. Kunikane, H. Yonetani, Y. Sakai: 'Fully Dynamic and Reconfigurable Optical Add/Drop Multiplexer on 0.8 nm Channel Spacing using AOTF and 32-wave Tunable lD Module'. In Opt. Fiber Commun. Conf., March 2000, Vol. 4, pp. 287–289
6 E.L. Adler, J.K. Slaboszewicz, C.K. Farnell, G.W. Jen: IEEE Trans. Ultrason. Ferroelectr. Freq. Control **37**, 215 (1990)
7 I. Belski, V. Sorokin: USSR Patent No. 1 298 549 (1987)
8 H. Mendis: *Investigation of Integrated Acousto-Optic Tunable Filters in Lithium Niobate*, Ph.D. thesis, RMIT University, 2001
9 K. Saithoh, M. Koshiba, Y. Tsuji: J. Lightwave Technol. **17**, 249 (1999)
10 A. Yariv, P. Yeh: *Optical Waves in Crystals* (Wiley, New York 1984)
11 F. Wehramann, C. Harizi, H. Herrmann, U. Rust, W. Sohler, S. Susanne: IEEE J. Sel. Top. Quantum Electron. **2**, 262 (1996)
12 M.B. Schulz, J.H. Matsinger: Appl. Phys. Lett. **20**, 367 (1972)
13 B.L. Heffner, D.A. Smith, J.E. Baran, A. Yi-Yan, K.W. Cheung: Electron. Lett. **24**, 1562 (1988)
14 D.A. Smith, J.J. Johnson: IEEE Photon. Technol. Lett. **3**, 923 (1991)
15 U. Rust: Modellierung Integriert Akustooptischer Bauelemente in Lithiumniobat, Ph.D. thesis, University of Paderborn, 1999
16 H. Herrmann, U. Rust, K. Schäfer: J. Lightwave Technol. **13**, 364 (1995)